*Molecular Physics*
Vol. 00, No. 00, Month 200x, 1–17

## RESEARCH ARTICLE

# Adsorption and interfacial phenomena of a Lennard-Jones fluid adsorbed in slit pores: DFT and GCMC simulations

J. M. Míguez[a], P. Gómez-Álvarez[a], M. M. Piñeiro[b], B. Mendiboure[c] and F. J. Blas[a] *

[a] *Laboratorio de Simulación Molecular y Química Computacional, CIQSO-Centro de Investigación en Química Sostenible and Departamento de Ciencias Integradas, Universidad de Huelva, 21007 Huelva, Spain*

[b] *Departamento de Física Aplicada, Facultade de Ciencias, Universidade de Vigo, 36310 Vigo, Spain*

[c] *UMR 5150-Laboratoire des Fluides Complexes et leurs Réservoirs, Université de Pau et des Pays de l'Adour, B. P. 1155 Pau, Cedex 64013, France*

(*Received 00 Month 200x; final version received 00 Month 200x*)

Confinement of fluids in porous media leads to the presence of solid-fluid interfaces that play a key role in many different fields. The experimental characterization of solid-fluid (SF) interfacial properties, in particular the surface tension, is challenging or not accessible. Theoretical and computational studies are hence indispensable but still scarce. In this work, we apply mean-field density-functional theory (DFT) to determine the surface tension and also density profile of a Lennard-Jones fluid in slit-shaped pores for realistic amounts of adsorbed molecules. We consider the pore walls to interact with fluid molecules through the well-known 10-4-3 Steele potential. The results are compared with those obtained from Monte Carlo simulations in the Grand Canonical Ensemble (GCMC) using the Test-Area method. We analyze the effect on the adsorption and interfacial phenomena of volume and energy factors, in particular the pore diameter and the ratio between solid-fluid and fluid-fluid dispersive energy parameters, respectively. The increase of either pore size or dispersive energy ratio unquestionably favors fluid adsorption. In regards to interfacial properties, density profile is considerably affected by the pore size but not by the relative strength of the energy, and the opposite for the solid-fluid surface tension. Overall, results from DFT and GCMC simulations were found to be comparable, which points to their reliability.

**Keywords:** Density Functional Theory, Monte Carlo simulation, Interfacial Tension, Test-Area, Adsorption

## 1. Introduction

Fluid adsorption in nanoporous materials is relevant to many fundamental and industrial applications involving separation, transport or catalysis processes. In this sense, a clear understanding of the microscopic behavior of the confined fluid at certain thermodynamic conditions is crucial. While the adsorption and diffusion of the guest molecules within the pores has been widely addressed, there is little information available on the solid-fluid (SF) interfacial properties, despite being in great part responsible for the thermodynamics and structure of the system [1, 2]. Unlike the liquid-vapor surface tension, SF surface tension is not experimentally accessible and its determination from a formal viewpoint entails mathematical difficulties related to the tensioral character of the pressure. Consequently, prior theoretical or computational studies [3, 4] focused on SF interfaces deal only with spherical

*Corresponding author. Email: felipe@uhu.es

ISSN: 0040-5167 print/ISSN 1754-2278 online

DOI: 10.1080/0040516YYxxxxxxxx
http://www.informaworld.com

molecules in pores of simple geometries, such as slit-shaped or cylindrical pores. On the one hand, there has been significant efforts in developing molecular-based theories of Statistical Mechanics to describe the behavior of inhomogeneous systems (coexisting phases). Among them, Density Functional Theory (DFT) [2, 5] is likely the most powerful approach to study confined fluids (SF interfaces). The intermolecular interactions within the fluid phase are covered by the intrinsic Helmholtz free energy, whereas molecular solid-fluid interactions are described through an external potential. The applied Helmholtz free energy functional mainly determines the accuracy of DFT predictions. We refer to recent reviews [6–8] for an overview of proposed Helmholtz free energy functionals and their applications. On the other hand, with the increasing computational power in the last decades, molecular simulation techniques [9] have become an alternative or fully complementary method to the theories. The computational evaluation of the local pressure tensor components has followed two routes: the mechanical method, based on the virial theorem [10, 11] and the thermodynamic method, based on the relationship between pressure and the Helmholtz (or Gibbs) free energy [12, 13]. Although the mechanical route [11] has been (and still is) the traditional method, the Test-Area (TA) technique [14], based on the thermodynamic definition, offers clear advantages of computational efficiency, ease of implementation, and generality. Recently, Míguez *et al.* [15] extended the Test-Area methodology of Gloor *et al.* [14] originally proposed to evaluate the surface tension of planar fluid-fluid interfaces in a computer simulation in the canonical ($NVT$) ensemble, to deal with SF surface tension of systems adsorbed on slit pores using the grand canonical ($\mu VT$) ensemble. This allows one to calculate in addition and simultaneously the density profiles and the adsorption loading. Besides, this method allows to determine a realistic value of the chemical potential $\mu$, which is kept constant during the simulation.

This work is aimed at comparing DFT and the TA methodology in Grand Canonical Monte Carlo (GCMC) simulations to account for adsorption and SF interfacial phenomena. This comparison constitutes the only way to test the predicting ability of these formal methods since the experimental determination of SF interfacial tension is not feasible, as commented above. We focus on spherical fluid molecules adsorbed in slit-like pores interacting through the well-known 10-4-3 Steele potential [16, 17]. Intermolecular interactions are described by a 12-6 Lennard-Jones potential in the GCMC simulations, and using the mean-field approximation for the attractive contribution to the Helmholtz free-energy in DFT. We have performed a systematic study of the adsorption loading, the density profiles and the surface tension for different pore sizes and dispersive energy parameters at fixed thermodynamic conditions of temperature and pressure. The rest of the paper is structured as follows. In section II, we describe the DFT formalism and the models and simulation details. The results are presented and discussed in section III. Finally, the main conclusions are detailed.

## 2. Methods

### 2.1. *Molecular simulations details*

We have studied adsorption and interfacial properties of a simple fluid in a pore using Grand Canonical Monte Carlo simulations ($\mu VT$). In particular, the geometry selected for this evaluation is a planar slit pore, composed by two non-structured flat parallel walls separated by a fixed distance, the pore width $H$. The fluid molecules are described through the classical Lennard-Jones (LJ) potential:

$$u_{ff}(r_{ij}) = 4\varepsilon_{ff}\left[\left(\frac{\sigma_{ff}}{r_{ij}}\right)^{12} - \left(\frac{\sigma_{ff}}{r_{ij}}\right)^{6}\right] \tag{1}$$

where $u_{ff}(r_{ij})$ is the intermolecular potential energy between particles $i$ and $j$, which depends only on the distance between the centres of the molecules $r_{ij} \equiv |\mathbf{r}_i - \mathbf{r}_j|$. The interactions are spherically truncated but not shifted at a given distance $r_c$. No long-range corrections have been applied and all the calculations are carried out for a cutoff distance of $r_c = 4\sigma_{ff}$. As it is well known, $\sigma_{ff}$ stands for the diameter of the molecular spherical core, and $\varepsilon_{ff}$ is the depth of the pairwise interaction potential. The subscript $ff$ stands for fluid-fluid molecular interactions. Also, the molecules interact with the confining walls. Among the extensive collection of models proposed in literature to account for solid-fluid molecular interactions, the so-called Steele 10–4–3 potential [16, 17] is very popular as it has been used to reproduce the interaction with realistic planar solid substrates as for instance graphite. This model considers that the atoms constituting the solid substrate are placed in layers separated by a distance $\Delta$, and placed parallel to the solid-fluid dividing surface. Each of the solid substrate atoms is supposed to interact with every individual fluid molecule through a LJ potential. With this setting, and considering that the atom density in each solid substrate layer is constant, the total interacting energy between a given molecule and one confining wall may be integrated, yielding the following expression:

$$u_{sf}(r) = 2\pi\varepsilon_{sf}\sigma_{sf}^2\rho_S\Delta\left[\frac{4}{10}\left(\frac{\sigma_{sf}}{z}\right)^{10} - \left(\frac{\sigma_{sf}}{z}\right)^{4} - \left(\frac{\sigma_{sf}^4}{3\Delta\,(z+0.61\Delta^3)}\right)\right] \tag{2}$$

where $z$ is the shortest distance from the centre of the molecule to the wall. The subscript $sf$ denotes in this case solid-fluid interactions. These characteristic interacting parameters are defined using the usual Lorentz-Berthelot rules, i.e., $\sigma_{sf} = \frac{1}{2}(\sigma_{ss} + \sigma_{ff})$, and $\varepsilon_{sf} = (\varepsilon_{ss}\,\varepsilon_{ff})^{1/2}$, where $\sigma_{sf}$ and $\varepsilon_{sf}$ are the crossed diameter and dispersive energy parameters for solid-fluid interactions, respectively. Typical graphite values of $\rho_S = 0.114$ and $\Delta = 3.35$ were selected, representing the solid substrate atom density within each layer, and interlayer spacing, respectively. Since the walls are oriented perpendicular to the $z$-axis and each molecule interacts with two walls, one located at $z = 0$ and the other one at $z = H$, the total solid-fluid interaction energy of a molecule placed at a distance $z$ from one of the walls is given by

$$U_{sf}^{TOT}(z) = u_{sf}(z) + u_{sf}(H - z) \tag{3}$$

In the calculations presented here, the range of both attractions has been considered to be the same, hence $\sigma_{ss} = \sigma_{ff}$, and the ratio $\varepsilon_{sf}/\varepsilon_{ff}$ has been tuned considering different values to explore the effect of the relative strength of both interactions on the confined fluid interfacial properties.

We have performed computer simulations in the Grand Canonical ($\mu VT$) ensemble. The simulation box is a parallelepiped of dimensions $L_x$, $L_y$ and $L_z$. The flat parallel walls were placed at $z = 0$ and $z = L_z = H$, which means that periodic boundary conditions do not apply along the $z$-axis.

The pore width plays an important role in any study concerning slab geometries, as it determines the capillarity effects induced by the confinement. In this work, different pore widths $L_z \equiv H$ were analized from $2\sigma_{ff}$ to $10\sigma_{ff}$.

All simulation runs were organized in cycles. For GCMC simulations, each cycle consisted in $N$ displacement movements and a molecule deletion or insertion trial. The type of movement was in every case selected at random according to their fixed probabilities, and the maximum displacements were tuned along the simulation to approach a 30% acceptance ratio. Initially, $N = 512$ Lennard-Jones molecules were placed inside the simulation box using a fcc grid. A typical run consisted of $5 \times 10^5$ equilibration cycles followed by a production stage of at least $2 \times 10^6$ cycles. During the production stage averages of the different interfacial properties were computed, including density profiles and interfacial tension. Density profiles along the $z$-axis were determined by dividing the box in 100 equal width slabs parallel to the confining surfaces. The uncertainties for the calculated interfacial tension values presented were determined using the block averaging technique, described elsewhere[9]. Interfacial tension of the system was calculated using TA methodology [14] recently extended to the Grand Canonical ($\mu VT$) ensemble[15]. Finally, adsorption was calculated as follows,

$$\Gamma = \int_0^H (\rho(z) - \rho_b) dz \tag{4}$$

where $\rho(z)$ represents the density profile of LJ fluid along the $z$-axis perpendicular to confining interfaces, and $\rho_b$ is the bulk density of the LJ fluid at the cited temperature and pressure conditions.

### 2.2. *Density Functional Theory (DFT)*

In this section we briefly recall the Density Functional Theory (DFT) formalism used to describe the SF interface of the studied confined fluids [5, 18] in planar slit pores.

As it is well known, the grand potential $\Omega[\rho(\mathbf{r})]$ of an inhomogeneous fluid is formulated as a functional of $\rho(\mathbf{r})$,

$$\Omega[\rho(\mathbf{r})] = A[\rho(\mathbf{r})] + \int d\mathbf{r}\rho(\mathbf{r})[V^{ext}(\mathbf{r}) - \mu] \tag{5}$$

where $A[\rho(\mathbf{r})]$ is the Helmholtz free energy functional, $V^{ext}(\mathbf{r})$ represents the external potential, and $\mu$ is the chemical potential for the bulk density ($\rho_b(\mathbf{r})$)

The Helmholtz free energy functional term is expressed as,

$$A[\rho(\mathbf{r})] = A^{ideal}[\rho(\mathbf{r})] + A^{HS}[\rho(\mathbf{r})] + A^{att}[\rho(\mathbf{r})] = A^{ideal}[\rho(\mathbf{r})] + A^{exc}[\rho(\mathbf{r})] \tag{6}$$

The ideal part, $A^{ideal}$, is the ideal-gas contribution, and it is an exactly known term given by,

$$A^{ideal}[\rho(\mathbf{r})] = k_B \int d\mathbf{r}\rho(\mathbf{r}) \left[\ln\{\rho(\mathbf{r})\Lambda^3\} - 1\right] \tag{7}$$

where $k_B$ is the Boltzmann constant and $\Lambda$ is the de Broglie thermal wavelength

of the molecules.

The hard-sphere free energy, $A^{HS}$, is treated non-locally using a weighted density approximation. Here, the Fundamental Measure Theory (FMT) [19, 20] has been selected because the free-energy reduces to the Carnahan-Starling equation of state in the bulk limit. This WDA provides six scalar and vector weighted densities $n_\alpha(\{(r)\})$,

$$n_\alpha(\mathbf{r}) = \int d\mathbf{r}' \rho(\mathbf{r}') w^{(\alpha)}(\mathbf{r}' - \mathbf{r}) \tag{8}$$

Here $\alpha = 0, 1, 2$, and 3, $v_1$ and $v_2$, and the weighted functions $w^{(\alpha)}(\mathbf{r})$.

The hard-sphere Helmholtz free energy is given by

$$A^{HS}[\rho(\mathbf{r})] = k_B T \int d\mathbf{r} \left[ \Phi^{HS_{(S)}}(\{n_\alpha(\mathbf{r})\}) + \Phi^{HS_{(v)}}(\{n_\alpha(\mathbf{r})\}) \right] \tag{9}$$

where $\Phi^{HS_{(S)}}\{n_\alpha(\mathbf{r})\}$ and $\Phi^{HS_{(v)}}\{n_\alpha(\mathbf{r})\}$ are respectively the scalar and vector terms of the reduced excess Helmholtz free energy density due to the hard core repulsion. They are calculated here according to the White bear version [21, 22].

The Helmholtz free energy functional due to the attractive contributions, $A^{att}$, is expressed according to the mean-field approximation by,

$$A^{att}[\rho(\mathbf{r})] = \frac{1}{2} \int d\mathbf{r} \rho(\mathbf{r}) \int d\mathbf{r}' \rho(\mathbf{r}')\, \phi^{att}(|\mathbf{r} - \mathbf{r}'|) \tag{10}$$

$\phi^{att}(r)$ is the attractive part of the intermolecular potential for particles separated a distance $r$ [23]. In particular, $\phi^{att}(r)$ is given here as

$$\phi^{att}(r) = \begin{cases} 0 & r \leq \sigma \\ u_{ij}^{LJ}(r) & r > \sigma \end{cases} \tag{11}$$

The equilibrium density distribution is the one that minimizes the grand potential functional, according to the variational principle,

$$\left. \frac{\partial \Omega[\rho(\mathbf{r})]}{\partial \rho(\mathbf{r})} \right|_{\rho(\mathbf{r}) = \rho_b(\mathbf{r})} = 0 \tag{12}$$

Finally, using the equation for the bulk in the asymptotic limit of a homogeneous fluid, the equilibrium density of the system may be formally written as,

$$\frac{\rho(\mathbf{r})}{\rho_b(\mathbf{r})} = \exp\left[ \frac{-V^{ext}(\mathbf{r}) + \mu_b^{ext}}{k_B T} - \int d\mathbf{r}' \sum_\alpha \frac{\partial \Phi(\mathbf{r})}{\partial n_\alpha(\mathbf{r}')} \frac{\partial n_\alpha(\mathbf{r}')}{\partial \rho(\mathbf{r})} - \int d\mathbf{r}' \rho(\mathbf{r}') \phi^{att}(|\mathbf{r} - \mathbf{r}'|) \right] \tag{13}$$

where $\mu_b^{ext}$ represents the bulk excess chemical potential, which can be obtained by the Boublík [24] and Mansoori *et al.* [25] expression, which is commonly referred to as the Boublík-Mansoori-Carnahan-Starling-Leland or BMCSL equation of state.

Specifically, for a fluid confined inside a planar slit pore where the walls are

oriented perpendicular to $z$-axis, one located at $z = 0$ and the other one at $z = H$, the external potential $V^{ext}(z)$ can be expressed as,

$$V^{ext}(z) = V_{sf}(z) + V_{sf}(H - z) \tag{14}$$

where $V_{sf}(z)$ is the 10-4-3 Steele potential [16] (see Eq. (2)).

The functional derivative of the attractive term $A^{att}(z)$, corresponding to the last contribution to the density profile in Eq. (14), can be written as,

$$\frac{\delta A^{att}(z)}{\delta \rho(z)} = \int d\mathbf{r}' \rho(\mathbf{r}') \phi^{att}(|\mathbf{r} - \mathbf{r}'|) = \int_0^H dz' \rho(z') u^{eff}(|z - z'|) \tag{15}$$

The effective intermolecular potential $u^{eff}$ is given by,

$$u^{eff}(|z - z'|) = \iint_{\mathcal{A}} dx' dy' \phi^{att}(\sqrt{x'^2 + y'^2 + |z - z'|^2}) \tag{16}$$

The last integral represents an average over the radial and angular variables in planes parallels to the pore and perpendicular to $z$-axis containing the interfacial area of the pore, $\mathcal{A}$. In practice, this integral may be solved by integrating in cylindrical coordinates.

Fluid-solid interfacial tension is calculated from,

$$\gamma = \frac{\Omega + PV}{2\mathcal{A}} \tag{17}$$

where $P$, $V$, and $\mathcal{A}$ represent the pressure in the bulk phase, volume, and interfacial area of the pore, respectively. The factor 2 in the previous equation takes into account the fact that the system has two fluid-solid interfaces, one at $z = 0$ and the other at $z = H$.

Finally, adsorption ($\Gamma$) is evaluated as described in the Molecular Simulation subsection.

## 3. Results and discussion

We have used the theoretical and computational methodologies explained in Sec. 2 to describe the adsorption and interfacial properties (density profiles and surface tension) of the Lennard-Jones fluid in a slit-like pore, as well as their dependence on the pore width and the dispersive energy ratio $\epsilon_{sf}/\epsilon_{ff}$. We worked with reduced quantities along this section, which are denoted by an asterisk, as usual. We choose the fluid-fluid sigma $\sigma_{ff}$ and dispersive energy $\epsilon_{ff}$ parameters as the units of length and energy, respectively. According to this, we define the following magnitudes: temperature $T^*=k_BT/\epsilon_{ff}$ , pressure $P^*= P\sigma_{ff}^3/\epsilon_{ff}$, chemical potential $\mu^*=\mu/\epsilon_{ff}$, density profile $\rho^*=\rho\sigma_{ff}^3$, surface tension $\gamma^*= \gamma\sigma_{ff}^2/\epsilon_{ff}$ , adsorption $\Gamma^*= \Gamma\sigma_{ff}^2$, pore size $H^*=H/\sigma_{ff}$ and distance from one of the walls, $z^*=z/\sigma_{ff}$. On the one hand, we examine the effect of pore size by considering $H^*$ values of 4, 5, 8 and 10 for the fixed ratio $\epsilon_{sf}/\epsilon_{ff} = 2.0$. On the other hand, the influence of the relative strength between the fluid molecules and the fluid-wall interactions was studied by setting

the $\epsilon_{sf}/\epsilon_{ff}$ ratio at 0.5, 1, 1.5, and 2.0 for a fixed pore width of $H^* = 8$. We selected $T^*$= 2.001 and $P^*$=0.136 since these working conditions corresponds to the usual conditions found in real tight gas reservoirs [26] . The chemical potential $\mu^*$ = -10.86(3) was determined from the fugacity, which is related to pressure. To this end, we used the Widom particle insertion method [27].

### 3.1. *Equilibrium adsorption*

Figures 1 and 2 show the results obtained from DFT and GCMC simulations concerning the adsorption loading of the LJ fluid in the slit pores. As it is evident, both the pore width and the dispersive energy ratio considerably affect the fluid adsorption. Specifically, the increase of $H^*$ and $\epsilon_{sf}/\epsilon_{ff}$ parameters leads to more available space within the pores and to stronger SF interactions (in relation to fluid-fluid interactions), respectively, which unquestionably favors adsorption. Our findings also reveal negligible dependence of the used methodology. They both predict virtually the same adsorption loadings at the tested conditions. Only subtle deviations appear for the most attractive pore walls (highest $\epsilon_{sf}/\epsilon_{ff}$ ratio). Tables 1 and 2 summarize adsorption results obtained from DFT and GCMC simulations.

### 3.2. *Interfacial properties*

For this system, where the molecules are located between two parallel walls, the $z$-axis is chosen perpendicular to the walls of the pore, and the $x$-axis and $y$-axis are parallel to the confining walls. With these assumptions, the equilibrium density profiles vary only along the $z$ coordinate, $\rho = \rho(z)$. They were hence computed from averages of the density histogram along this direction over the production stage. Interestingly, the results from both methods, DFT and GCMC simulations, are again fully consistent. As expected, the density profiles are symmetrical to the pore center with oscillatory behavior. The system develops dense layers near the SF interfaces, approximately at a distance $\sigma$ from each wall, regardless of the pore size or energy parameters. Also, density peaks of lower intensity appear, which indeed depend on both volumetric and energetic factors. Figure 3 accounts for $\rho(z)$ variations induced by the pore width (at $\epsilon_{sf}/\epsilon_{ff}$ =2). As it can be noticed, for the largest pore sizes considered ($H^*$=8 and $H^*$=10), two minor layers are formed close to the dense layers, and a nearly flat density profile is observed around the center of the pore. This denotes negligible SF interactions, and thus bulk-like behavior for the molecules located in this central region. This is consistent with strong interactions between the walls and molecules if compared to fluid-fluid interactions. As a consequence of decreasing pore size, these absorbed molecules approximate the pore center and a single centered layer, apart from the dense films on the planar walls, is observed for $H^*$=4. This is the expected density profile for even narrower pores. Results as a function of $\epsilon_{sf}/\epsilon_{ff}$ (at $H^*$=8) are given in Figure 4. In all cases, the system exhibits two layers near each pore wall, at distance about one and two ($\sigma_{ff}$), respectively. The layers closer to the pore walls are unquestionably denser. As $\epsilon_{sf}/\epsilon_{ff}$ ratio increases, and so the SF interactions become relatively stronger, the height of these density peaks consistently increases. A comparison between Figures 3 and 4 reveals that density profiles are considerably less affected by the dispersive energy ratio than by the pore width.

Once the structural behavior of the LJ fluid inside the slit pore is well characterized in terms of the density profiles, we present and discuss the surface tension $\gamma^*$ of the systems. Figure 5 and Table 1 present the values obtained using both methods for different pore widths at $\epsilon_{sf}/\epsilon_{ff}$ =2. We found interfacial tension $\gamma^*$

values to be ∼-30 for $H^*$=5, 8 and 10, and considerably more negative (larger in absolute value) for $H^*$= 4. Particularly, it takes a value close to $\gamma^*$=-45 for this lowest pore size. Overall, SF cohesion energy increases with increasing the density of the adsorbed phase, and SF surface tension of adsorbed layers at sufficiently large pores is expected not to change significantly with the pore size. Our results are fully consistent with these statements, and we can conclude that the 'threshold' value of pore size $H^*$ from which surface tension is virtually kept constant is between 4 and 5. This affirmation is more evident from the results obtained by DFT.

Table 2 and Figure 6 show the SF interfacial tension when the relative strength $\epsilon_{sf}/\epsilon_{ff}$ is changed for a fixed $H^*$=8. Three obvious conclusions can be drawn. First, the interfacial tension becomes more negative with increasing $\epsilon_{sf}/\epsilon_{ff}$ energy ratio from 0.5 up to 2.0. The relatively higher value for $\epsilon_{sf}$ leads to more cohesive SF interactions. Specifically, an almost linear dependence of surface tension with $\epsilon_{sf}/\epsilon_{ff}$ ratio is observed. Second, surface tension varies from about -2.5 (at $\epsilon_{sf}/\epsilon_{ff}$=0.5) to -30 (at $\epsilon_{sf}/\epsilon_{ff}$=2.0). This range of $\gamma^*$ values is notably broader than that found for the tested pore sizes (Fig. 5). Therefore, we can state that this interfacial property is relatively more sensitive to the dispersive energy ratio. Finally, the values of surface tension obtained by both methods are fully consistent, except for the highest considered ratio $\epsilon_{sf}/\epsilon_{ff}$=2. The difference for the surface tension at this ratio likely arises from the difference for molecular adsortion (Fig. 2). Since this is indeed the ratio value selected to study the effect of the pore size, the deviations between both methods in Figures 1 and 5 are expected to be reduced for lower $\epsilon_{sf}/\epsilon_{ff}$ ratios. In fact, the difference between both theoretical approaches in the case were $\epsilon_{sf}/\epsilon_{ff} = 2$ should probably to the highly non-ideal situation. The usual Lorentz-Berthelot combining rules approximation represents a crude approach that loses some accuracy in these circunstances. Indeed, this may affect also the DFT calculations, producing results that may not be as nice as when mixtures of more alijke interactinf segments are examined using this approach.

## 4. Conclusions

We have determined the solid-fluid interfacial properties of spherical Lennard-Jones molecules adsorbed in slit-like pores interacting through the well-known 10-4-3 Steele intermolecular potential using Density Functional Theory (DFT) and molecular simulation (GCMC). We examined the influence of the ratio between solid-fluid and fluid- fluid dispersion interaction parameters, and also of the pore size on the interfacial phenomena. As expected, the adsorption of the LJ fluid in the slit pore is enhanced by an increase of either pore size or the dispersive energy ratio. The obtained density profiles reveal that the structure of the layers adsorbed in the pore is considerably affected by the pore size, but nearly independent on the dispersive energy ratio. In regard to the solid-fluid interfacial tension, it increases in absolute value as the energy ratio increases (the fluid attraction to the walls is relatively enhanced), and as the pore size decreases. More particularly for the latter case, surface tension was found notably larger (in absolute value) for $H^*$=4 than for the remaining tested pore sizes, for which a virtually constant value of surface tension is observed, especially when using DFT. Hence, for pore width $H^*$ values beyond 4 or 5 no significant changes of the surface tension of the system studied are expected (for the targeted energy ratio).

Overall, we found a satisfactory agreement between results predicted by DFT and GCMC simulations, even for surface tension, which is one of the most sensitive properties to subtle differences in approximations made in the theories. We

have thus proved that the used Fundamental Measure Theory is able to describe accurately the SF interfacial tension for a number of pore sizes and dispersive energy ratios. This is not the case for the highest tested energy ratio (highly attractive pore walls), for which we found somewhat evident discrepancies for this property between both methods. The detailed analysis of this particular difference deserves to be the subject of a further study.

## Acknowledgments

The authors would like to acknowledge helpful discussions with A. I. Moreno-Ventas Bravo. We also acknowledge Centro de Supercomputación de Galicia (CESGA, Santiago de Compostela, Spain) and MCIA (Mésocentre de Calcul Intensif Aquitain) of the Universités de Bordeaux and Pau et Pays de l'Adour (France), for providing access to computing facilities, and Ministerio de Economía y Competitividad through Grants with references FIS2015-68910-P and FIS2015-71749-REDT and Ministerio de Economía, Industria y Competitividad through Grant with reference FIS2017-89361-C3-1-P, all three co-financed by EU FEDER funds. Further financial support from Junta de Andalucía and Universidad de Huelva is also acknowledged.

## References

[1] D. Henderson, *Fundamentals of Inhomogeneous Fluids* (Dekker, New York, 1992).
[2] H. T. Davis, *Statistical Mechanics of Phases, Interfaces, and Thin Films* (VCH, Weinheim, 1996).
[3] J. R. Henderson and F. van Swol, Mol. Phys. **51**, 991 (1984).
[4] P. E. Brumby, H. H. Wensink, A. J. Haslam, and G. Jackson., Langmuir **33**, 11754 (2017).
[5] R. Evans, *Density Functionals in the Theory of Nonuniform Fluids. In Fundamentals of Inhomogeneous Fluids* (Dekker, New York, 1992).
[6] H. Löwen, J. Phys. Condens. Matter **46**, 11897 (2002).
[7] J. Wu, AIChE Journal. **52**, 1169 (2006).
[8] J. Wu and Z. Li, Annu. Rev. Phys. Chem. **58**, 85 (2007).
[9] D. Frenkel and B. Smit, *Understanding Molecular Simulation* (Academic Press, 2002).
[10] J. G. Kirkwood and F. P. Buff, J. Chem. Phys. **17**, 338 (1949).
[11] J. H. Irving and J. G. Kirkwood, J. Chem. Phys. **18**, 817 (1950).
[12] L. L. Lee, *Molecular Thermodynamics of Non-ideal Fluids* (Butterworth, Boston, 1988).
[13] J. S. Rowlinson and B. Widom, *Molecular Theory of Capillarity* (Claredon Press, 1982).
[14] G. J. Gloor, G. Jackson, F. J. Blas, and E. de Miguel, J. Chem. Phys. **123**, 134703 (2005).
[15] J. M. Míguez, M. M. Piñeiro, A. I. M. V. Bravo, and F. J. Blas, J. Chem. Phys. **136**, **114707** (2012).
[16] W. A. Steele, *The Interaction of Gases with Solid Surfaces*, chap. 4 (Pergamon, 1974).
[17] W. A. Steele, Surf. Sci. **36**, 317 (1973).
[18] J. P. Hansen and I. R. McDonald, *Theory of Simple Liquids, 3rd Edition* (Academic Press, London, 2006).
[19] Y. Rosenfeld, J. Chem. Phys. **89**, 4272 (1988).
[20] Y. Rosenfeld, D. Levesque, and J.-J. Weis, J. Chem. Phys. **92**, 6818 (1990).
[21] R. Roth, R. Evans, A. Lang, and G. Kahl, J. Phys. Condens. Matter **14**, 12063 (2002).
[22] Y.-X. Yu and J. Wu, J. Chem. Phys. **117**, 10156 (2002).
[23] J. A. Barker and D. J. Henderson, J. Chem. Phys. **47**, 2856 (1967).
[24] T. Boublík, J. Chem. Phys. **53**, 471 (1970).
[25] G. A. Mansoori, N. F. Carnahan, K. E. Starling, T. W. Leland, and J. Chem. Phys. **54**, 1523 (1971).
[26] J. M. Míguez, M. C. dos Ramos, M. M. Piñeiro, and F. J. Blas, J. Phys. Chem B **115**, 9604 (2011).
[27] B. Widom, J. Chem. Phys. **19**, 563 (1963).

Table 1. Solid-fluid interfacial tension and adsorption of LJ molecules adsorbed on slit-like pores of different pore widths $H^*$ and dispersive energy ratio $\varepsilon_{sf}/\varepsilon_{ff} = 2.0$. $\gamma^*_{TA-\mu VT}$ and $\gamma^*_{DFT}$ are the interfacial tensions obtained from the TA method in the grand canonical ensemble and from the Density Functional Theory, respectively. $\Gamma^*_{muVT}$ and $\Gamma^*_{DFT}$ represent the adsorptions obtained in these pores using Grand Canonical Monte Carlo simulation method and Density Functional Theory, respectively.

| $H^*$ | $\gamma^*_{TA-\mu VT}$ | $\gamma^*_{DFT}$ | $\Gamma^*_{\mu VT}$ | $\Gamma^*_{DFT}$ |
|---|---|---|---|---|
| 4 | −43.67(7) | −44.61 | 2.59 | 2.40 |
| 5 | −33.1(5) | −30.28 | 3.05 | 2.86 |
| 8 | −27.2(5) | −29.30 | 3.35 | 3.26 |
| 10 | −28.2(5) | −29.25 | 3.35 | 3.26 |

Table 2. Solid-fluid interfacial tension and adsorption of LJ molecules adsorbed on slit-like pores of pore width $H^* = 8$ and different dispersive energy ratios $\varepsilon_{sf}/\varepsilon_{ff}$. $\gamma^*_{TA-\mu VT}$, $\gamma^*_{DFT}$,$\Gamma^*_{\mu VT}$, $\Gamma^*_{DFT}$ represent the same as in the caption of Table I.

| $\varepsilon_{sf}/\varepsilon_{ff}$ | $\gamma^*_{TA-\mu VT}$ | $\gamma^*_{DFT}$ | $\Gamma^*_{\mu VT}$ | $\Gamma^*_{DFT}$ |
|---|---|---|---|---|
| 0.5 | −2.49(2) | −2.57 | 1.30 | 1.36 |
| 1.0 | −10.19(6) | −9.90 | 2.25 | 2.27 |
| 1.5 | −20.0(2) | −19.11 | 2.89 | 2.84 |
| 2.0 | −27.2(5) | −29.30 | 3.35 | 3.26 |

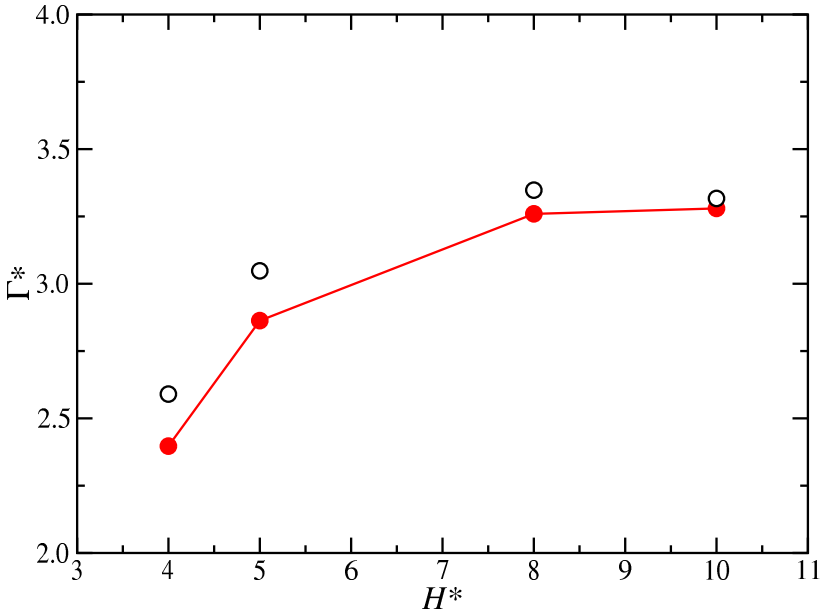


Figure 1. Adsorption loading of a LJ fluid in a slit pore at $T^*$ = 2.001 and $\mu^*$ = -10.86(3) for different pore widths $H^*$ and $\epsilon_{sf}/\epsilon_{ff}$ =2.0 from DFT calculations (red line) and GCMC simulations (open black symbols).

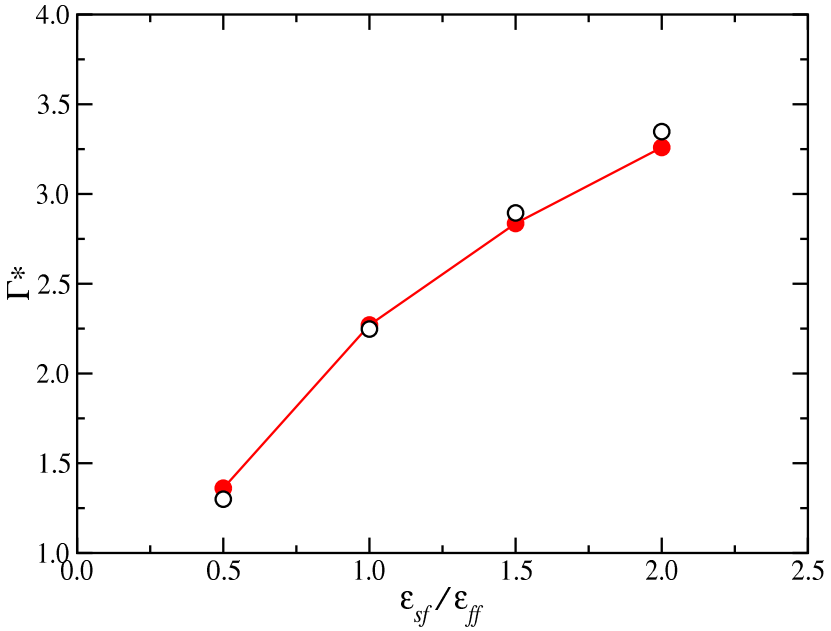


Figure 2. Adsorption loading of a LJ fluid in a slit pore at $T^*$ = 2.001 and $\mu^*$ = -10.86(3) for different energy strengths $\epsilon_{sf}/\epsilon_{ff}$ and $H^*$=8 from DFT calculations (red line) and GCMC simulations (open black symbols).

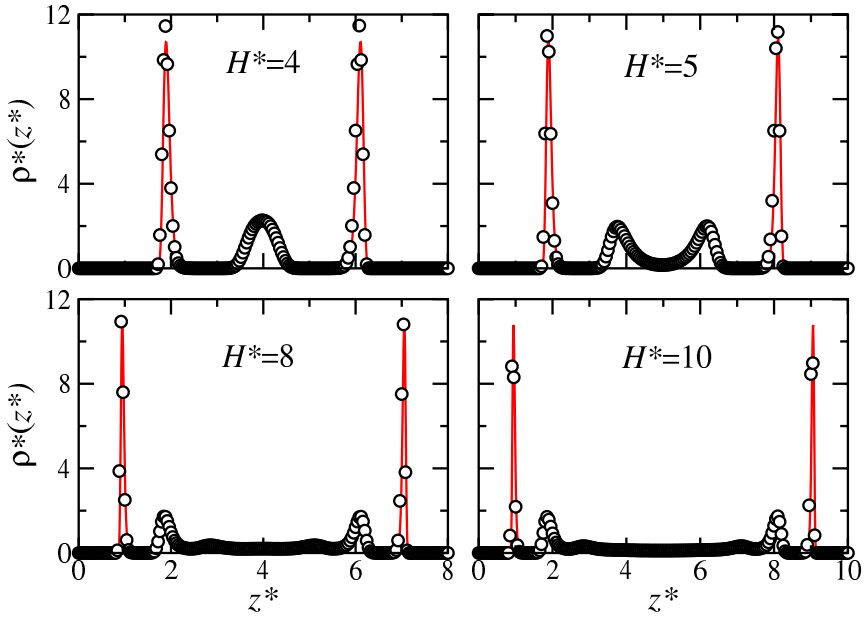


Figure 3. Density profiles $\rho(z)$ of a LJ fluid in slit pore at $T^* = 2.001$ and $\mu^* = -10.86(3)$ for different pore widths $H^*$ and $\epsilon_{sf}/\epsilon_{ff} = 2.0$ from DFT calculations (red lines) and GCMC simulations (open black symbols).

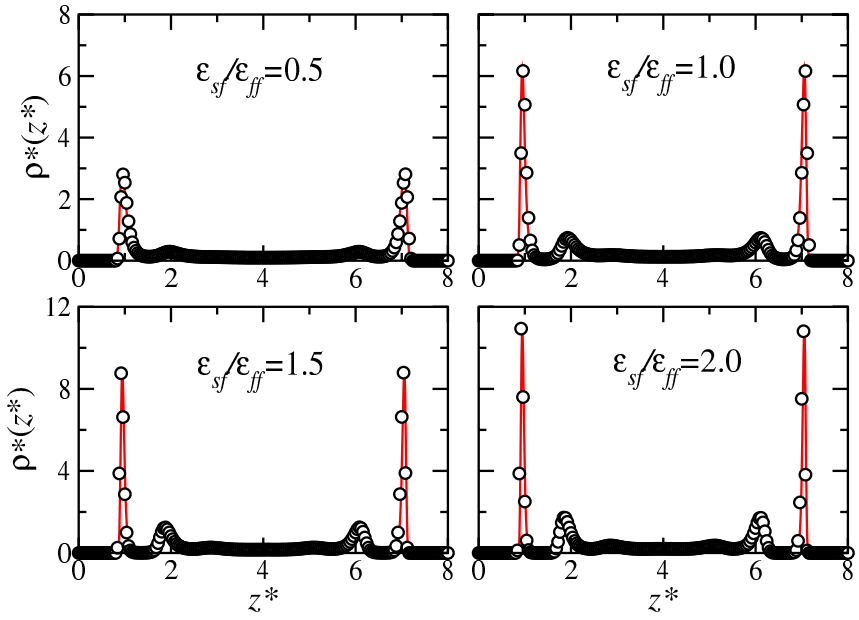


Figure 4. Density profiles $\rho(z)$ of a LJ fluid in slit pore at $T^*$ = 2.001 and $\mu^*$ = -10.86(3) for different energy strengths $\epsilon_{sf}/\epsilon_{ff}$ and $H^*$=8 from DFT calculations (red lines) and GCMC simulations (open black symbols).

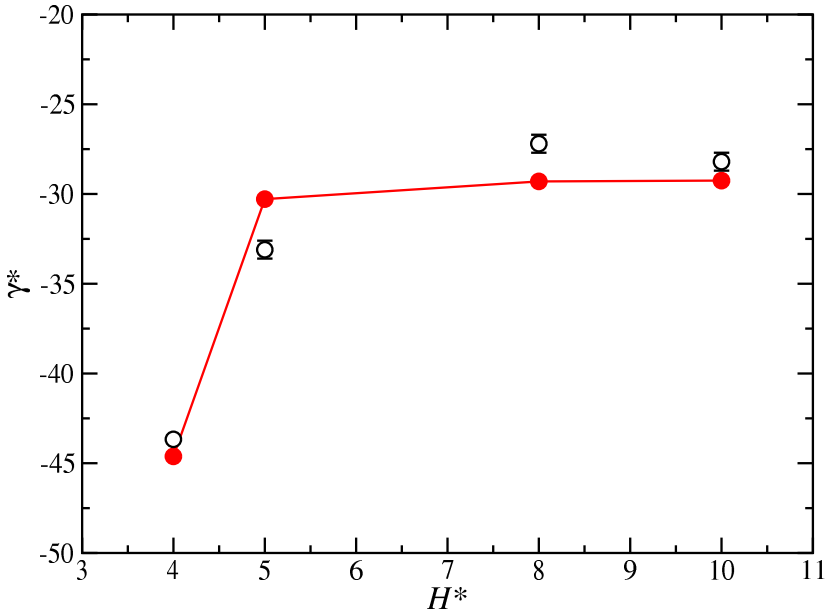


Figure 5. Solid-fluid interfacial tension $\gamma^*$ of a LJ fluid in slit pore at $T^* = 2.001$ and $\mu^* = -10.86(3)$ for different pore widths $H^*$ and $\epsilon_{sf}/\epsilon_{ff}$=2.0 from DFT calculations (red line) and GCMC simulations using TA method (open black symbols). Error bars for data obtained from simulations are depicted.

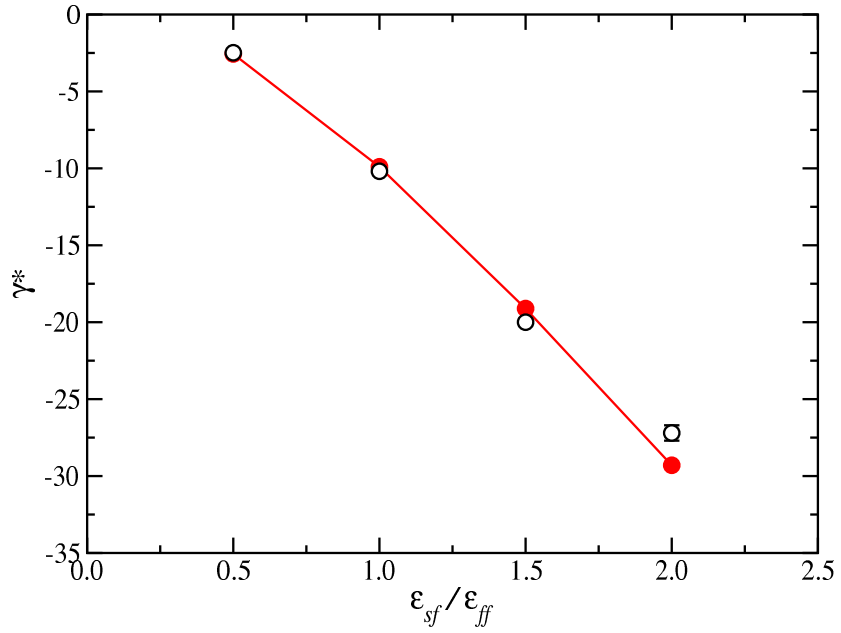


Figure 6. Solid-fluid interfacial tension $\gamma^*$ of a LJ fluid in slit pore at $T^* = 2.001$ and $\mu^* =$ -10.86(3) for different energy strengths $\epsilon_{sf}/\epsilon_{ff}$ and $H^* =$8 from DFT calculations (red line) and GCMC simulations using TA method (open black symbols).